

UV laser-induced desorption mechanism analyzed through two-layer alkali halide samples

F. A. Fernández-Lima,^{1,2} C. R. Ponciano² and E. F. da Silveira^{2*}

¹ Instituto Superior de Tecnologías y Ciencias Aplicadas, Havana, Cuba

² Physics Department, Pontifícia Universidade Católica, Rua Marques de São Vicente 225, 22452-900 Rio de Janeiro, Brazil

Received 6 September 2006; Accepted 15 October 2007

Time of flight-mass spectrometry (TOF-MS) is used to analyze positive and negative desorbed ions generated by UV laser ablation of several alkali (X) halide (Y) salts. Most of the observed desorbed cluster ions have the structure $(XY)_nX^+$ or $(XY)_nY^-$. Their desorption yields decrease as $\exp(-kn)$, where $k \approx 2$ for both series, suggesting that the neutral component $(XY)_n$ plays the dominant role in the desorption process. Mass spectrum measurements were performed for compound samples in which two salts (out of CsI, RbI, KBr, KCl and KI) are homogeneously mixed or disposed in two superposed layers. The detection of small new ion species and large cluster ions of the original salts supports the scenario that the uppermost layers are completely atomized while deep layers are emitted colder and fragmented: It is proposed that ns-pulsed laser induced desorption of ionic salts occurs via two sequential mechanisms: (1) ejection of cations and anions in the hot plume, followed by recombination into new cluster ions and (2) ejection of relatively cold preformed species originated from deep layers or from periphery of the irradiated region. Copyright © 2007 John Wiley & Sons, Ltd.

KEYWORDS: laser ablation; alkali halide; cluster ion; TOF

INTRODUCTION

The mechanism of energy deposition and energy transfer from the optically absorbing components to the transparent components is a basic phenomenon in laser physics.^{1–3} The models of material removal by laser irradiation may be classified into two major categories: (1) ablation models which are based either on the idea of collective ejection of a volume of material due to rapid nonequilibrium phase transition^{4,5} or on a critical pressure gradient,^{4,6,7} and (2) quasi-thermal desorption models that are based on different descriptions of the rapid surface vaporization process.^{4,6,8–11}

We have previously reported a thermal ablation model to describe the dynamics of the cesium ions created by UV laser in the first stages of their temporal evolution¹² by two mechanisms¹³: one representing the energy absorption/deposition and another in which it is determined the probability of occurrence of atomic species recombination during the expansion of the high density and highly ionized cloud. In particular, alkali halide cluster ions have been observed previously^{14–18} and its formation is still under investigation.

In the current work, time of flight-mass spectrometry (TOF-MS)¹⁸ is pursued to study the ions generated by laser ablation/vaporization of several alkali halide salts: XY (where X = Cs, Rb, or K and Y = I, Br, or Cl). A series of

target combinations of two salts were prepared and ablated, producing cluster ions whose yield analysis is expected to contribute to the understanding of the laser desorption mechanism.

EXPERIMENT

Sample preparation and characterization

CsI, RbI, KI, KBr, and KCl powders ($\geq 99.5\%$ purity) were evaporated on a stainless steel sample holder of the spectrometer. All the single-species polycrystalline films were grown by deposition in an evaporation chamber at a pressure of 10^{-5} mbar. Seven composite targets, i.e. composed by two salts on the same holder, were prepared in the following way:

1. Two homogeneous targets, referred to hereafter as 'mixed' CsI + KBr or RbI + KCl samples, were prepared by using the standard dried droplet method from a 1 : 1 mixture of the two salts in equimolar aqueous solutions.
2. Five structured targets, referred to, hereafter, as 'non-mixed' samples, were prepared by evaporating sequentially two overlaid layers of two salt powders on the stainless steel holder: KBr/CsI, CsI/KBr, KCl/RbI, RbI/KCl and 2*RbI/KCl. The 2*RbI/KCl target was made by evaporation of the double amount of RbI material over a previously evaporated KCl layer. The typical thickness of each layer was ~ 600 nm, much larger than the interface region (few nanometers), guaranteeing the nonmixed character of the target.

*Correspondence to: E. F. da Silveira, Physics Department, Pontifícia Universidade Católica, Rua Marques de São Vicente 225, 22452-900 Rio de Janeiro, Brazil. E-mail: enio@vtdg.fis.puc-rio.br

The UV absorption coefficient was measured in an HP8452A Hewlett–Packard Spectrophotometer for an aqueous solution of each salt. The optical density is $A = \varepsilon_{\text{MA}} \times C \times d$, where ε_{MA} is the molar absorption coefficient, C is the molar concentration and d is the optical distance inside the quartz sample cell. Table 1 presents the molar absorption coefficients for 337 nm (or 3.7 eV) UV obtained for pure salts in water, the melting points and cohesive energies of the same compounds in a crystalline form.^{19–21} Note that the ε_{MA} values range as: $\varepsilon_{\text{MA}}(\text{CsI}) > \varepsilon_{\text{MA}}(\text{RbI}) \gg \varepsilon_{\text{MA}}(\text{KI}) \gg \varepsilon_{\text{MA}}(\text{KBr}) > \varepsilon_{\text{MA}}(\text{KCl})$. The inspection of Table 1 shows that there is a monotonic correspondence among the three sets of values, which means that CsI is the material that absorbs the most UV laser energy per mole centimeter and has the lowest melting point temperature. Therefore, it is expected that the desorption yield of CsI should be higher than the others and so on.

In the current experiments, four salts grouped into two pairs of alkali halides were chosen, with the criterion that each pair should be composed of one salt that absorbs the UV laser strongly (or has a lower melting point) and another one that absorbs it weakly. The four targets prepared were: CsI on/under KBr, since $\varepsilon_{\text{MA}}(\text{CsI}) \gg \varepsilon_{\text{MA}}(\text{KBr})$, and RbI on/under KCl, since $\varepsilon_{\text{MA}}(\text{RbI}) \gg \varepsilon_{\text{MA}}(\text{KCl})$.

Mass spectrometry analysis

The MS experiments were performed in a BRUKER/BIFLEX III two-acceleration region linear mass spectrometer, which uses a 337 nm nitrogen laser of 3 ns full width at half maximum (FWHM).¹⁸ To guarantee reproducibility, three different spots were examined on two distinct samples; for each spot, the mass spectrum was acquired with an average of 10 laser shots of $I = 1.9$ and 0.89 GW/cm^2 for the RbI + KCl and CsI + KBr targets, respectively. In the case of the 'nonmixed' samples, the positive and negative spectra were acquired in a virgin site with a single laser shot, creating a hole throughout both salts and removing the material once. The laser intensities of $I = 4.6$ and 6.4 GW/cm^2 were employed for the first pair KBr–CsI (targets KBr/CsI and

CsI/KBr) and the second pair KCl–RbI (targets KCl/RbI, RbI/KCl and 2^*RbI/KCl), respectively, to force the complete local target evaporation.

RESULTS AND DISCUSSION

The mass spectrum of each alkali halide salt ($\sim 600 \text{ nm}$ thick) was measured as a reference. Next, the mass spectra of 'composite' samples were analyzed and classified according to their structural composition in: (1) 'mixed' (forming a homogenous mixture of the two anions and the two cations) and (2) 'nonmixed' (formed by two structured layers, i.e. constituting an alkali halide species deposited over another).

Laser ablation/vaporization of pure alkali halide samples

The laser irradiation of each (pure) alkali halide salt produces a series of cluster ions, denoted by $(\text{XY})_n\text{X}^+$ or $(\text{XY})_n\text{Y}^-$ where: XY is the alkali halide analyzed (i.e. CsI, RbI, KBr, KCl and KI), X^+ is the cation (Cs^+ , Rb^+ , and K^+), and Y^- is the anion (I^- , Br^- and Cl^-), respectively. TOF peaks for $n > 4$ are not observed over the background level. This behavior is observed for both the positive and negative series, in agreement with previously reported results for CsI and RbI samples.^{13,18} The measured values of the slope parameter k_m (as well as $k = k_m M$) are presented in Table 2, corresponding to the average of several laser intensities, ranging from $I = 0.89$ to 4.61 GW/cm^2 .

The two major findings are: (1) the yields of the negative cluster ions are about one order of magnitude lower than that of the positive ion ones, and (2) the shape of positive and negative cluster ion distributions are about the same, i.e. a decreasing exponential distribution with a slope parameter $k \approx 2$ (Table 2). This result suggests that the recombination in the cluster formation is a general process for desorption of all the alkali halide species. Alkali halide cluster ions produced by electrospray ionization also show an exponential behavior on n , but with $k \sim 0.4$.¹⁶

Table 1. The molar absorption coefficients, melting points and cohesive energies of the studied alkali halide compounds in their crystalline form

	CsI	RbI	KI	KBr	KCl
$\varepsilon_{\text{MA}} (\text{mol}^{-1} \text{ cm}^{-1})$	371	143	8	1	0.6
Melting Point ($^{\circ}\text{C}$)	621	642	723	730	776
Cohesive energy (eV/atom pair)	−5.6	−6.30	−6.49	−6.86	−7.18

Table 2. Cluster ion slope parameters k_m and k of the 'pure' alkali halide species.

$Y(I, m) = Y_0(I) \exp(-k_m m) = Y_0'(I) \exp(-kn)$, where I is the laser intensity, m is the cluster mass and k_m (or k) is the slope parameter

Series	$k_m (\times 10^{-3})$	k	Series	$k_m (\times 10^{-3})$	k
$(\text{KCl})_n\text{K}^+$	27 ± 4	2.3 ± 0.3	$(\text{KCl})_n\text{Cl}^-$	18 ± 4	1.8 ± 0.4
$(\text{KBr})_n\text{K}^+$	20 ± 4	2.5 ± 0.5	$(\text{KBr})_n\text{Br}^-$	12 ± 4	1.7 ± 0.5
$(\text{KI})_n\text{K}^+$	11 ± 3	1.8 ± 0.5	$(\text{KI})_n\text{I}^-$	13 ± 3	2.2 ± 0.5
$(\text{RbI})_n\text{Rb}^+$	12 ± 3	2.4 ± 0.6	$(\text{RbI})_n\text{I}^-$	8 ± 3	1.4 ± 0.5
$(\text{CsI})_n\text{Cs}^+$	9 ± 2	2.0 ± 0.4	$(\text{CsI})_n\text{I}^-$	7 ± 2	1.3 ± 0.4

Some scenarios for the cluster emission process should be considered:

Preformed cluster mechanism

Since the ionic (poly)crystalline target is constituted by a periodic structure $(X^+Y^-)_m$, it should fracture into the distribution of $(XY)_n$, $(XY)_nX^+$ and $(XY)_nY^-$ fragments. Assuming a low number of collisions in the plume, the distribution of the detected ions should be very similar to the distribution of the ionic fractured pieces.

Atomization-recombination mechanism

Collisions inside the hot expanding plume favor, besides electron capture, the reactions $X^+ + Y^- \rightarrow XY$ and $X + Y \rightarrow XY$. In a second stage, cooler, the recombination $(XY)_{n-1} + XY \rightarrow (XY)_n$ produces larger neutral clusters. During or at the end of this second stage, the ion attachment processes $(XY)_{n-1} + X^+ \rightarrow (XY)_nX^+$ and $(XY)_{n-1} + Y^- \rightarrow (XY)_nY^-$ also occur. It is expected that the distributions of neutral, positive and negative cluster ions should have similar shapes.

These two scenarios are not mutually exclusive: the second one may occur at the very hot target surface while the first one may occur afterwards when the laser absorption in target is greatly attenuated by the growing plume generated at the superficial layers. The temperature of the target surface is always cooler than that of the front part of the plume by orders of magnitude.¹² This situation leads to a temperature gradient in the plume that, in combination with the plume

density gradient (\sim constant during the laser pulse), will favor either the first or the second mechanism. A method to explore this model is using targets formed by thin multilayer films to identify the origin of the observed cluster ions.

Laser ablation/vaporization of composite alkali halide samples

If the hypothesis that the laser ablation produces a homogeneous and high density ionized gas formed by atomic species is assumed, then a very similar mass spectrum should be obtained for any chemical composition of the target, provided that the average stoichiometry is the same.

Figure 1(a) and (b) present the positive mass spectra for the 'mixed' CsI + KBr and RbI + KCl samples, respectively. For the laser intensity used, the relative yields for the atomic cations Cs^+ , K^+ and Rb^+ are huge and saturate (at 250 a.u. for the current data acquisition setup). A large number of peaks is observed, corresponding to cluster ions generated by the recombination among the two cations and the two anions of each group.

In Figs 2 and 3, the four positive mass spectra of the 'nonmixed' samples of KBr–CsI and KCl–RbI are presented for both figures: (a) represents the case in which the lower UV absorbent is deposited over the stronger one, and (b) represents the inverse geometry (inverse order of the layers). The desorption yields for all positively and

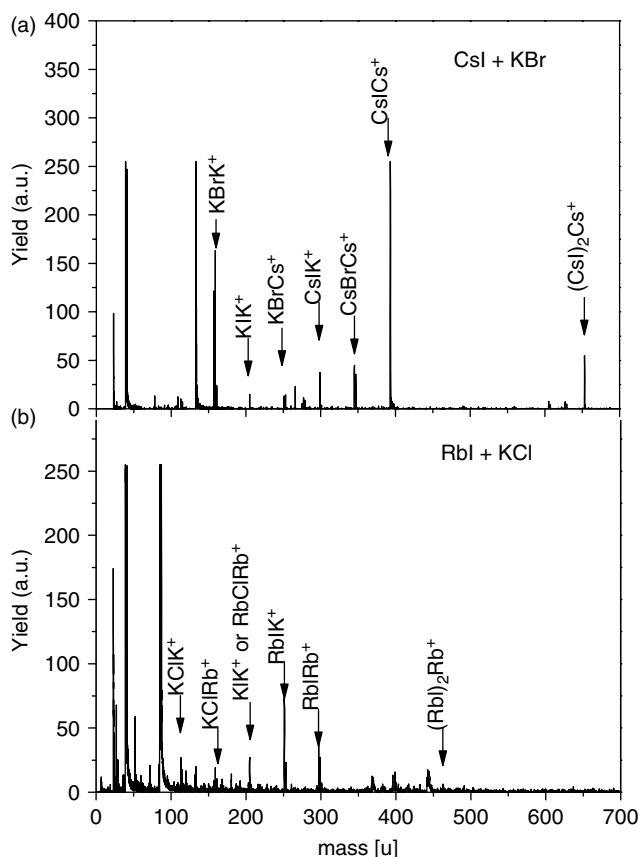


Figure 1. Positive ion mass spectra for the 'mixed' (a) CsI + KBr and (b) RbI + KCl targets. Yield values are relative and saturate at $Y = 250$.

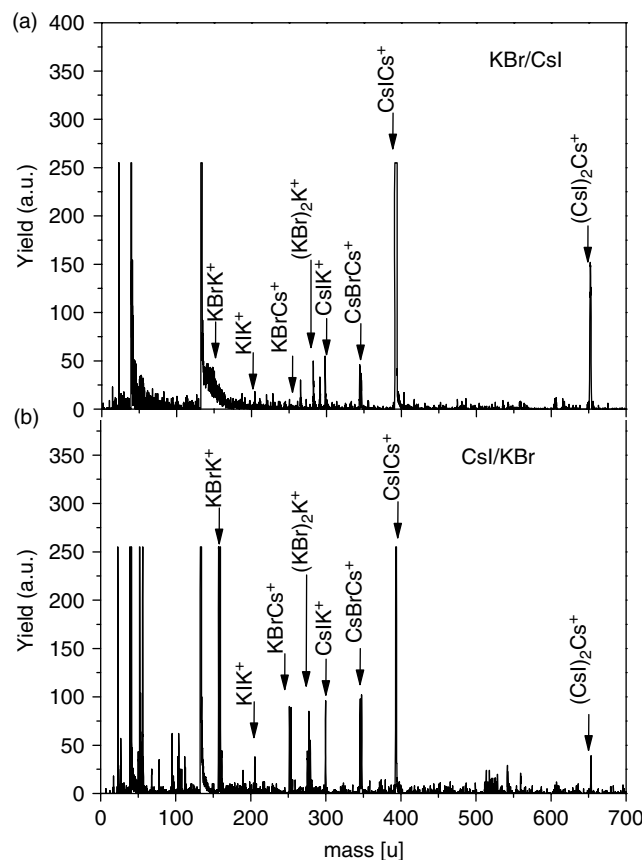


Figure 2. Positive ion mass spectra for the 'nonmixed' (a) KBr/CsI and (b) CsI/KBr targets. KBr/CsI means that KBr was deposited on a CsI thin film. Yield values are relative and saturate at $Y = 250$.

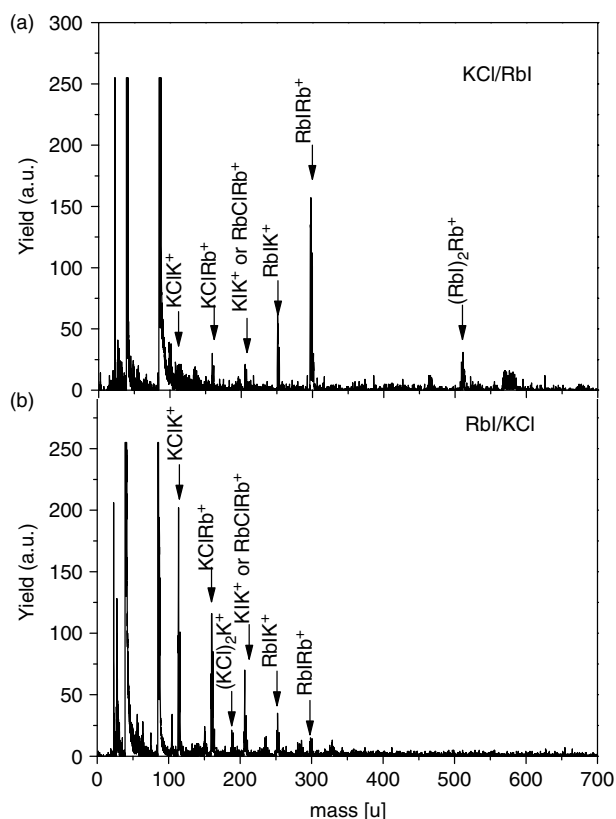


Figure 3. Positive ion mass spectra for the 'nonmixed' (a) KCl/RbI and (b) RbI/KCl targets. See comments in Fig. 2.

negatively charged species, emitted from the 'mixed' and 'nonmixed' samples, are shown in Tables 3–5.

Yield distribution of the cluster series

Since the yield distributions of the alkali halide cluster ions decrease exponentially, a simple way to characterize them is to determine the yield of the first member, Y_1 , and the slope parameter k_m (or k). The relative yields of the atomic cations are high and differ strongly according to the sample's homogeneity: they have not been analyzed here since lower laser intensities are required. In Table 3, the first member yields are presented in such a way that, per sample, the sum of the yields relative to all the chemically possible combinations of the atoms in three-element cluster is normalized to 100%. For clarity, only four out of six possible combinations are shown in the Table 3, but all data (not normalized) are presented in Tables 4 and 5.

For the structured targets (nonmixed samples), the observation of a mass peak corresponding to a nonpreformed species is obviously an evidence of the recombination process. On the other hand, the observation of a peak due to the original salt does not necessarily characterize a preformed species: a complete dissociation followed by recondensation into the same compound might have occurred. As a reference, the analysis of 'pure' samples is useful in this case.

Regarding the CsI–KBr samples (first group), it is interesting to observe in Table 3a that:

1. For the mixed (homogeneous) sample, the $(\text{CsI})\text{Cs}^+$ have the highest yield.

Table 3. Left side: a) Normalized desorption yields Y_1 of the first members of the cluster series $(\text{CsI})_n\text{Cs}^+$ and $(\text{KBr})_n\text{K}^+$, for the three sample configurations: "mixed" CsI + KBr; "non-mixed" KBr/CsI and "non-mixed" CsI/KBr targets. b) idem for the RbI and KCl salts; there are two RbI thicknesses for the RbI/KCl target. For each sample, the sum of the six yields is 100%; note that the two highest values (bold characters) are mostly in the diagonal and correspond to preformed species. Right side: The cluster series slope parameters; typical absolute errors are $\pm (0.002 \text{ to } 0.003)$

(a)	Normalized Y_1 (%)		Yield distribution			Sample
	CsI	KBr	cluster	$k_m (\times 10^{-3})$	k	
Cs	71.1	1.6	$(\text{CsI})_n \text{Cs}^+$	9	2.3	Mixed
K	5.2	14.7	$(\text{KBr})_n \text{K}^+$	23	2.7	
Cs	78.2	0.8	$(\text{CsI})_n \text{Cs}^+$	5	1.3	KBr/CsI
K	5.7	6.9	$(\text{KBr})_n \text{K}^+$	35	4.1	
Cs	11.5	18.0	$(\text{CsI})_n \text{Cs}^+$	9	2.3	CsI/KBr
K	6.9	47.0	$(\text{KBr})_n \text{K}^+$	16	1.9	
<hr/>						
(b)	RbI	KCl				
Rb	18.1	11.1	$(\text{RbI})_n \text{Rb}^+$	16	3.4	Mixed
K	30.2	18.9	$(\text{KCl})_n \text{K}^+$	20	1.5	
Rb	57.3	6.8	$(\text{RbI})_n \text{Rb}^+$	10	2.1	KCl/RbI
K	21.9	7.3	$(\text{KCl})_n \text{K}^+$	26	1.9	
Rb	2.5	28.4	$(\text{RbI})_n \text{Rb}^+$	10	2.1	RbI/KCl
K	3.9	57.8	$(\text{KCl})_n \text{K}^+$	23	1.8	
Rb	1.0	3.6	$(\text{RbI})_n \text{Rb}^+$	13	2.8	2*RbI/KCl
K	14.6	31.0	$(\text{KCl})_n \text{K}^+$	26	1.9	

2. For the KBr/CsI sample (i.e. KBr is the uppermost layer), the yield of the 'preformed' *underneath* species $(\text{CsI})\text{Cs}^+$ is one order of magnitude higher than that of the 'preformed' $(\text{KBr})\text{K}^+$ and than those of the not-preformed $(\text{CsI})\text{K}^+$ and $(\text{KBr})\text{Cs}^+$ species.
3. For the CsI/KBr sample (i.e. CsI is the uppermost layer), again the 'preformed' *underneath* species $(\text{KBr})\text{K}^+$ is most abundant.

For the mixed sample, the laser is not homogeneously absorbed in the target: a higher abundance of free ions occurs where the UV is more absorbed, namely by the CsI link. This explains why $(\text{CsI})\text{Cs}^+$ presents the highest desorption yield. Moreover, Cs has the smallest ionization potential (3.89 eV) compared to Rb (4.18 eV) and K (4.34 eV).²¹

For the structured samples, it is clear that the salt *underneath* produces the largest number of cluster ions. These experiments evidence that these clusters are 'preformed', belonging to a colder part of the plume (closer to the target surface). Furthermore, it is observed that the yields of the species of the uppermost layer are relatively small and comparable to that of the recombined clusters: this is also experimental evidence that such clusters are formed by recondensation in the very hot plume (farther from the target surface). Both results corroborate on the expected behavior that a strong temperature gradient is created down the interior of the target: the surface material is completely atomized, homogenized and partially recondensed, whereas

Table 4. Desorption yields of the $(XY)_n X^+$ and $(XY)_n Y^-$ ion clusters emitted from the ‘mixed’ CsI + KBr and from the ‘nonmixed’ KBr–CsI targets. Each pair cation/anion cluster is represented in the left column by $(XY)_n X^+/Y^-$. Right: the yields for the target configurations: (1) homogeneous, (2) the KBr over the CsI film and (3) the inverse position. Values in brackets: the real values should be higher (saturated experimental signals)

Detected cluster				Yield		
Pre-formed $(XY)_n$	New $(XY)_n$	X^+/Y^-	Cluster mass [u]	Mixed	KBr/CsI	CsI/KBr
KBr		K^+/Br^-	157/197	265/10	182/10	(2808)/(2228)
		Cs^+/I^-	251/245	29/10	22/29	1078/792
CsI		K^+/Br^-	299/339	94/6	149/134	416/87
		Cs^+/I^-	393/387	1280/180	(2040)/(2295)	690/161
-	KI	K^+/I^-	205/293	31/21	40/779	592/649
	CsBr	Cs^+/Br^-	345/291	100/2	173/2	384/94
(KBr) ₂		K^+/Br^-	275/315	11/2	3/1	422/98
		Cs^+/I^-	369/363	3/0	0/0	63/57
(CsI) ₂		K^+/Br^-	559/599	6/6	39/20	52/14
		Cs^+/I^-	653/647	122/9	581/541	81/12
KBr	KI	K^+/I^-	323/411	6/0	1/2	81/19
	CsBr	Cs^+/Br^-	463/409	2/0	0/7	48/2
CsI	KI	K^+/I^-	465/553	1/1	0/44	52/21
	CsBr	Cs^+/Br^-	605/551	12/2	30/11	43/0
(KBr)(CsI)		K^+/Br^-	417/457	1/1	21/5	45/3
		Cs^+/I^-	511/505	3/0	4/5	59/4
-	(KI) ₂	K^+/Br^-	371/411	2/0	2/2	174/19
	(CsBr) ₂	Cs^+/I^-	557/551	3/1	3/11	24/0

the underneath material may be ejected colder resembling the original structure of the target surface.

These considerations were tested on new measurements with the second alkali halide group, RbI–KCl, whose normalized yields of the first cluster, Y_1 , are displayed in Table 3b. For the mixed sample, RbI, KCl, KI and RbCl are formed in the solution. Since RbI and KI absorb more UV radiation than KCl and RbCl, the yields for the $(XI)X^+$ three element cluster ions are likely to present the highest abundance, as observed experimentally. For the two nonmixed samples, results confirm those obtained for the CsI–KBr group: the ‘preformed’ underneath species in the KCl/RbI and RbI/KCl samples are the most abundant. Regarding the 2*RbI/KCl sample (the RbI layer in this sample was twice thicker), the temperature gradient effect makes the combination into new species, which corresponds to almost the 50% of the emitted ions (mass 205, not shown in Table 3a, but included in Table 5). Again, for the double RbI layer, an incomplete mixing occurs in the plasma, since the underneath layer yield is one order of magnitude higher than that of the uppermost layer.

The yield enhancement of the ‘preformed’ underneath species is also observed through the analysis of the slope parameter k (see values in Table 3). An equivalent method of performing the same analysis is by inspection of the yields of five-atom clusters (the second cluster member). Tables 4 and 5 show that the second cluster yields of the ‘preformed’ species follow the same tendency of the first cluster: the underneath ‘preformed’ species has the largest yield.

Yields of the species produced by atomization–recombination

Starting from the two alkali halide pairs, all the possible combinations among them in cluster formation are observed in measurements, as shown in Tables 4 and 5. Although the cluster ion yields decrease when the nuclearity increases, the recombination is still observed in large cluster ions.

For the case of the first group of the ‘nonmixed’ CsI–KBr samples, the formation of the $(KI)_n K^+$ and $(CsBr)_n Cs^+$ series illustrates the occurrence of the recombination process. Their formation does not show any influence of the ‘preformed’ alkali halides CsI and KBr. Note in Table 4 that this result is also confirmed for the second group of the ‘nonmixed’ samples, KCl–RbI, for both positive and negative spectra.

CONCLUSIONS

Mass spectrometry of pure ionic salts reveals that the abundance distributions of positive and negative cluster ions are fitted quite well by an exponential function. This fact leads to the conclusion that the laser desorption mechanism is the same for both species and that the formation and ejection of neutral structure of the cluster, $(XY)_n$, dominate the process. On the other hand, such information does not disclose the nature of the mechanism and measurements with multilayer targets were performed for tracing the initial sites of the desorbed species.

The ‘preformed’ underneath-layer cluster ion species $(CsI)Cs^+$ in the KBr/CsI system is about one order of magnitude higher than the yield of: (1) $(KBr)K^+$ species

Table 5. Desorption yields of the 'mixed' RbI + KCl and 'nonmixed' KCl + RbI targets. Same comments made for Table 3. In the case of a mass coincidence of two possible species, the values were marked with an asterisk '*'. The yields correspond to the mass of the lightest isotope of each element

Detected cluster				Yield				
Pre-formed (XY) _n	New (XY) _n	X ⁺ /Y ⁻	Cluster mass [u]	Mixed	KCl/RbI	RbI/KCl	2*RbI/KCl	
KCl		K ⁺ /Cl ⁻	113/109	112/17	141/539	659/335	398/186	
		Rb ⁺ /I ⁻	159/201	66/16	132/11	324/21	46/36	
RbI		K ⁺ /Cl ⁻	251/247	179/6	424/8	45/13	187/13	
		Rb ⁺ /I ⁻	297/339	107/34	1107/1823	29/67	14/400	
-	KI	K ⁺ /I ⁻	205/293	127*/30	127*/775	83*/19	635*/1366	
	RbCl	Rb ⁺ /Cl ⁻	205/155	127*/3	127*/30	83*/22	635*/300	
(KCl) ₂		K ⁺ /Cl ⁻	187/183	25/2	17/51	27/43	81/6	
		Rb ⁺ /I ⁻	233/275	18/1	14/5	23/8	13/3	
(RbI) ₂		K ⁺ /Cl ⁻	463/459	16/3	63/10	0/1	13/345	
		Rb ⁺ /I ⁻	509/551	4/0	121/72	3/0	1/1	
KCl	KI	K ⁺ /Cl ⁻	279/229	12/1	10/43	8/38	16/5	
	RbCl	Rb ⁺ /I ⁻	279/367	12/2*	10/2*	8/6*	16/0*	
RbI	KI	K ⁺ /Cl ⁻	417/367	24/2*	13/2*	5/6*	19/0*	
	RbCl	Rb ⁺ /I ⁻	417/505	24/1	13/52	5/2	19/51	
(KCl)(RbI)		K ⁺ /Cl ⁻	325/321	76/0	9/9	20/9	4/5	
		Rb ⁺ /I ⁻	371/413	31*/1	5*/1	9*/0	44*/3	
		(KI) ₂	K ⁺ /Cl ⁻	371/367	31*/2	5*/2*	9*/6	44*/0
		(RbCl) ₂	Rb ⁺ /I ⁻	325/367	8/2*	9/2*	20/6*	0/0*

emitted from the upper layers; and (2) not preformed species such CsBrCs⁺ or KIK⁺. Similar results occur for negative cluster ions and for the inverse system CsI/KBr. These findings are considered as strong evidence of emission of 'cold' residues of the fractured solid, that is, preformed cluster ions coming from underneath layers. Since the yield of the species initially at the uppermost layer is lower than the underneath layer one and is comparable to the yield of the recombined species, it is also concluded that there is recondensation in the hot atomic plasma into the same species or into new species if mixed with other ions coming from the lower layers. This scenario is in agreement with the description that the laser shot generates a strong temperature gradient inside the target, atomizing the heated surface material in a first stage and then desorbing the underneath material as 'preformed' colder clusters. The same argument can be used to postulate that 'preformed' clusters are emitted from the periphery of the laser spot, where ionized and relatively 'cold' chunks survive the desorption process.

The inhomogeneous-sample experiment is proposed as a strategy for analyzing quantitatively the contribution of different mechanisms occurring in laser desorption and determining spatially the domains of each one. More sophisticated targets such as organic/inorganic layers, multilayers samples or even cylindrical layers coaxial with the laser beam can be designed for comprehensive conclusions.

Acknowledgements

The authors would like to acknowledge the Brazilian Agencies CNPq, Faperj and CLAF for their support.

REFERENCES

- Fournier I, Tabet JC, Bolbach G. Irradiation effects in MALDI and surface modifications – part I: sinapinic acid monocrystals. *International Journal of Mass Spectrometry* 2002; **219**: 515.
- Karas M, Bahr U, Fournier I, Gluckmann M, Pfenninger A. The initial-ion velocity as a marker for different desorption-ionization mechanisms in MALDI. *International Journal of Mass Spectrometry* 2003; **226**: 239.
- Karas M, Gluckmann M, Schafer J. Ionization in matrix-assisted laser desorption/ionization: singly charged molecular ions are the lucky survivors. *Journal of Mass Spectrometry* 2000; **35**: 1.
- Vertes A, Gijbels G. In *Laser Ionization Mass Analysis*, Vertes A, Gijbels R, Adams F (eds). Wiley: New York, 1993; 127.
- Kelly R, Miotello A. Comments on explosive mechanisms of laser sputtering. *Applied Surface Science* 1996; **96–98**: 205.
- Johnson RE. In *Large Ions: their Vaporization, Detection and Structural Analysis*, Baer T, Ng CY, Powis I (eds). Wiley: New York, 1996; 49.
- Braun R, Hess P. Time-of-flight investigation of infrared laser-induced multilayer desorption of benzene. *Journal of Chemical Physics* 1993; **99**: 8330.
- Piuz F. CsI-photocathode and RICH detector. *Nuclear Instruments and Methods in Physical Research Section A* 1996; **371**: 96.
- Fahler S, Krebs HU. Calculations and experiments of material removal and kinetic energy during pulsed laser ablation of metals. *Applied Surface Science* 1996; **96–98**: 61.
- Rosen DI, Mitteldorf J, Pugh G. Coupling of pulsed 0.35 – μm laser radiation to aluminum alloys. *Journal of Applied Physics* 1982; **53**: 3190.
- Breskin A. CsI UV photocathodes: history and mystery. *Nuclear Instruments and Methods in Physical Research Section A* 1996; **371**: 116.
- Fernández-Lima F, Collado VM, Ponciano CR, Farenzena LS, Pedrero E, da Silveira EF. Laser ablation of CsI analyzed by delayed extraction. *Applied Surface Science* 2003; **217**: 202.
- Collado VM, Fernández-Lima FA, Ponciano CR, Marco Antonio Chaer Nascimento, Velazquez L, da Silveira EF. Laser induced

- formation of CsI ion clusters analyzed by delayed extraction time-of-flight mass spectrometry. *Physical Chemistry Chemical Physics* 2005; **7**: 1971.
- Morgan TG, Rabrenovic M, Harris FM, Beynon JH. Investigation of the relative stability of positive alkali halide cluster ions generated by fast atom bombardment. *Organic Mass Spectrometry* 1984; **19**: 315.
 - Twu YJ, Conover CWS, Yang YA, Bloomfield LA. Alkali-halide cluster ions produced by laser vaporization of solids. *Physical Review B* 1990; **42**: 5306.
 - Wang G, Cole RB. Solvation energy and gas-phase stability influences on alkali metal cluster ion formation in electrospray ionization mass spectrometry. *Analytical Chemistry* 1998; **70**: 873.
 - Kimura Y, Saito Y, Nakada T, Kaito C. Spontaneous mixing of binary alkali halide crystal by successive evaporation. *Physica E* 2002; **13**: 11.
 - Fernández-Lima FA, Ponciano CR, Fonseca Filho HD, Pedrero E, Chaer Nascimento MA, da Silveira EF. UV laser induced desorption of CsI and RbI ion clusters. *Applied Surface Science* 2006; **252**: 8171.
 - Tosi MP. In *Solid State Physics*, vol. 16, Seitz F, Turnbull D (eds). Academic press: New York, 1964; 54.
 - Satpathy S. Electron energy bands and cohesive properties of CsCl, CsBr, and CsI. *Physical Review B* 1986; **33**: 8706.
 - Lide DR (ed). *Handbook of Chemistry and Physics*. CRC Press: Boca Raton, New York, London, Tokyo; 1995.